inter.noise
HAMBURG 2016

An Arnoldi reduction applied to wave propagation to model railway track vibrations

R. Cettour-Janet[1], A. Barbarulo, F. Létourneaux, G. Puel
Laboratoire MSSMat, Ecole Centrale Paris/CNRS UMR 8579, Grande Voie des Vignes, 92290 Châtenay-Malabry, France
SYSTRA, 72 Rue Henry Farman, 75015 Paris, France

ABSTRACT
With metropolis and transport grid densification, the result of acoustic impact assessment has a pivotal role in rail network expansion. Rolling noise is an important source. To simulate this latter, railway track vibration model is needed. In this paper, vibrational response of the railway track is simulated taking into account the infinite dimension of the rail, its cross-section deformation and the periodic support is developed. Waveguide finite element method (WFEM) allows to create a generic element. This latter is coupled with Floquet theorem to simulate the periodic part of the track. This technique produces instabilities and numerical problems which imposed an adaptive algorithm. They are solved by using second-order Arnoldi method (SOAR). This reduction eliminates critical values and create an orthogonal basis. Firstly, the model is describe. Then its stability is shown. Finally numerical results are compared with experimental data.

Keywords: Railway Track, Vibration, waveguide finite element method Second order Arnoldi reduction

1. INTRODUCTION

With metropolis and transport grid densification, the result of acoustic impact assessment has a pivotal role in rail network expansion. Indeed, for railway neighbours, a main problem is the pass-by train noise. When the train runs between 80 and 300 km/h [1], the main noise source is the rolling noise. To evaluate this latter and to reduce it, the vibrational response of the railway track is needed.

On the one hand, analytic methods [2] (beams, mass, spring ...) are not valid at high frequency because of the need to include cross-section deformation. On the other hand, the infinite dimension in the longitudinal direction imposes a truncation of the 3D FEM methods. Moreover, when increasing the frequency, 3D FEM computation time becomes unacceptable.

Waveguide finite element method (WFEM) can also be used [3–6]. It allows to model the infinite dimension of the rail and its cross-section deformation. However, models cited above don't take into account the periodic support and consequently the pin pin frequency.

In [7, 8] , a model taking into account the infinite dimension of the rail, its cross-section deformation and the periodic support is developed. The WFEM is used to create a generic element. This latter is a longitudinal rail section attached at the two ends to a half sleeper (cf. Fig. 1). The infinite part of the railway track is simulated connecting a generic element i to an element i+1. However, this connection generates numerical problems imposing an adapted algorithm. This problem has been addressed in [7, 8] but instability and error in low frequency limit its effectiveness.

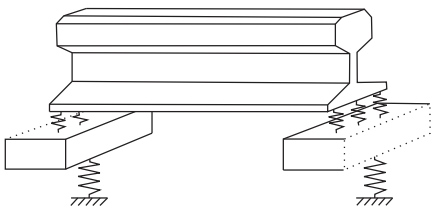

Fig. 1: Scheme of the periodic element - longitudinal rail section and its half sleepers

[1]email: rcettourjanet@systra.com

This paper suggests the use of a more suited algorithm to provide the missing model stability: the Second Order Arnoldi Reduction (SOAR).

Firstly, the model is described. Then its stability is shown. Lastly, numerical results are compared with experimental data.

2. WAVEGUIDE BASED ON FINITE ELEMENT METHOD FOR RAIL VIBRATION

2.1 Waveguide finite element method

The waveguide finite element method (WFEM) [9–18] is used to model an elastic body with a constant cross section lying on a plane and an infinite dimension in its orthogonal direction. In this article, the longitudinal direction ($\overrightarrow{e_z}$) of the rail is supposed infinite.

WFEM assumes that displacement $\mathbf{u}(x,y,z,t)$ can be split in two parts $\boldsymbol{\phi}(x,y)$ and $q(z,t)$.

$\boldsymbol{\phi}$ symbolizes mode shape of the cross section in the three directions ($\boldsymbol{\phi}_x, \boldsymbol{\phi}_y$ and $\boldsymbol{\phi}_z$). It is approximated thanks to finite element formulation. $\phi = \sum_i^{N_{elt}} \boldsymbol{N}_i(x,y)\,\boldsymbol{\phi}_i^{FE}$. $\boldsymbol{N}(x,y)$ and $\boldsymbol{\phi}^{FE}$ are respectively the shape functions and the generalized coordinates.

q symbolizes waves propagation in the z-direction, it is a scalar.

Finally, the displacement is the sum of the shape functions times the propagating part :

$$\boldsymbol{u}(x,y,z,t) = \sum_{j=1}^{N_m} \boldsymbol{\phi}_j(x,y)\, q_j(z,t) \tag{1}$$

where N_m is the number of calculated modes.

Rail is an isotropic material. Consequently, strains and stresses are defined by the following formulas : $\epsilon_{\mathrm{ij}} = \frac{1}{2}\left(\frac{\partial \mathrm{u_j}}{\partial \mathrm{x_i}} + \frac{\partial \mathrm{u_i}}{\partial \mathrm{x_j}}\right)$ and $\boldsymbol{\sigma} = \lambda \mathrm{tr}(\boldsymbol{\epsilon}) + 2\mu\boldsymbol{\epsilon}$. λ and μ are Lamé constants.

Moreover, the generic element (cf. Fig. 1) is a piece of rail supported by a half sleeper at the both ends. Consequently, external forces are the force generated by the sleeper ($\boldsymbol{F}_{sleeper}$), and the stress fields ($\boldsymbol{G}(0)$ and $\boldsymbol{G}(L)$) applied to both ends sections.

Using the hypothesis (1), the virtual work principle leads to the following equations :

$$\begin{cases} \left[\left[\mathbf{B}_0 - \omega^2\mathbf{M}\right] + \left[\mathbf{B}_1 - \mathbf{B}_2\right]k - \mathbf{B}_3 k^2\right]\boldsymbol{\phi}^{EF} = 0 \\ \mathbf{G}_p(0) = -\mathbf{B}_2\mathrm{q}(0) - \mathbf{B}_3\frac{\partial \mathrm{q}(0)}{\partial z} - \frac{1}{2}\mathbf{A}_p(0) \\ \mathbf{G}_p(L) = \mathbf{B}_2\mathrm{q}(L) + \mathbf{B}_3\frac{\partial \mathrm{q}(L)}{\partial z} - \frac{1}{2}\mathbf{A}_p(L) \end{cases} \tag{2}$$

With

$$\begin{aligned} \mathbf{B}_0 = \sum_{i=1}^{N_{elt}} \int_{\mathrm{A}_i} & (\lambda+2\mu)\left[\frac{\partial \boldsymbol{N}_{\mathrm{xi}}^{*\mathrm{T}}}{\partial \mathrm{x}}\frac{\partial \boldsymbol{N}_{\mathrm{xi}}}{\partial \mathrm{x}} + \frac{\partial \boldsymbol{N}_{\mathrm{yi}}^{*\mathrm{T}}}{\partial \mathrm{y}}\frac{\partial \boldsymbol{N}_{\mathrm{yi}}}{\partial \mathrm{y}}\right] \\ & + \lambda\left[\frac{\partial \boldsymbol{N}_{\mathrm{xi}}^{*\mathrm{T}}}{\partial \mathrm{x}}\frac{\partial \boldsymbol{N}_{\mathrm{yi}}}{\partial \mathrm{y}} + \frac{\partial \boldsymbol{N}_{\mathrm{yi}}^{*\mathrm{T}}}{\partial \mathrm{y}}\frac{\partial \boldsymbol{N}_{\mathrm{xi}}}{\partial \mathrm{x}}\right] \\ & + \mu\left[\frac{\partial \boldsymbol{N}_{\mathrm{yi}}^{*\mathrm{T}}}{\partial \mathrm{x}} + \frac{\partial \boldsymbol{N}_{\mathrm{xi}}^{*\mathrm{T}}}{\partial \mathrm{y}}\right]\left[\frac{\partial \boldsymbol{N}_{\mathrm{yi}}}{\partial \mathrm{x}} + \frac{\partial \boldsymbol{N}_{\mathrm{xi}}}{\partial \mathrm{y}}\right] \\ & + \mu\left[\frac{\partial \boldsymbol{N}_{\mathrm{zi}}^{*\mathrm{T}}}{\partial \mathrm{x}}\frac{\partial \boldsymbol{N}_{\mathrm{zi}}}{\partial \mathrm{x}} + \frac{\partial \boldsymbol{N}_{\mathrm{zi}}^{*\mathrm{T}}}{\partial \mathrm{y}}\frac{\partial \boldsymbol{N}_{\mathrm{zi}}}{\partial \mathrm{y}}\right]\mathrm{dA}_i \end{aligned}$$

$$\mathbf{B}_1 = \sum_{i=1}^{N_{elt}} \int_{\mathrm{A}_i} \lambda\left[\frac{\partial \boldsymbol{N}_{\mathrm{xi}}^{*\mathrm{T}}}{\partial \mathrm{x}}\boldsymbol{N}_{\mathrm{zi}} + \frac{\partial \boldsymbol{N}_{\mathrm{yi}}^{*\mathrm{T}}}{\partial \mathrm{y}}\boldsymbol{N}_{\mathrm{zi}}\right] + \mu\left[\frac{\partial \boldsymbol{N}_{\mathrm{zi}}^{*\mathrm{T}}}{\partial \mathrm{x}}\boldsymbol{N}_{\mathrm{xi}} + \frac{\partial \boldsymbol{N}_{\mathrm{zi}}^{*\mathrm{T}}}{\partial \mathrm{y}}\boldsymbol{N}_{\mathrm{yi}}\right]\mathrm{dA}_i$$

$$\mathbf{B}_2 = \sum_{i=1}^{N_{elt}} \int_{\mathrm{A}_i} \lambda\left[\boldsymbol{N}_{\mathrm{zi}}{}^{*\mathrm{T}}\frac{\partial \boldsymbol{N}_{\mathrm{yi}}}{\partial \mathrm{y}} + \boldsymbol{N}_{\mathrm{zi}}{}^{*\mathrm{T}}\frac{\partial \boldsymbol{N}_{\mathrm{xi}}}{\partial \mathrm{x}}\right] + \mu\left[\boldsymbol{N}_{\mathrm{xi}}{}^{*\mathrm{T}}\frac{\partial \boldsymbol{N}_{\mathrm{zi}}}{\partial \mathrm{x}} + \boldsymbol{N}_{\mathrm{yi}}{}^{*\mathrm{T}}\frac{\partial \boldsymbol{N}_{\mathrm{zi}}}{\partial \mathrm{y}}\right]\mathrm{dA}_i$$

$$\mathbf{B}_3 = \sum_{i=1}^{N_{elt}} \int_{\mathrm{A}_i} (\lambda + 2\mu)\, \boldsymbol{N}_{\mathrm{zi}}^{*\mathrm{T}} \boldsymbol{N}_{\mathrm{zi}} + \mu \left[\boldsymbol{N}_{\mathrm{yi}}^{*\mathrm{T}} \boldsymbol{N}_{\mathrm{yi}} + \boldsymbol{N}_{\mathrm{xi}}^{*\mathrm{T}} \boldsymbol{N}_{\mathrm{xi}} \right] \mathrm{dA}_i$$

$$\mathbf{M} = \sum_{i=1}^{N_{elt}} \int_{\mathrm{A}_i} \rho \boldsymbol{N}_i^{*\mathrm{T}} \boldsymbol{N}_i \mathrm{dA}_i$$

N_{xi},N_{yi} and N_{zi} are the shape function of the i^{th} element in the x, y and z direction. A_i is the area of the i^{th} element. N_{elt} is the number of element.

In (2), the first equation represents waves in the free rail. The other ones represent stresses at the two ends of the element.

2.2 Stationary solution of the free rail

Equation (2) is a quadratic eigenvalue problem (QEP).

$$\left[\left[\mathbf{B}_0 - \omega^2 \mathbf{M} \right] + \left[\mathbf{B}_1 - \mathbf{B}_2 \right] k - \mathbf{B}_3 k^2 \right] \boldsymbol{\phi}^{EF} = 0 \Leftrightarrow \left[\mathbf{K}_0 + \mathbf{K}_1 k + \mathbf{K}_2 k^2 \right] \boldsymbol{\phi}^{EF} = 0 \tag{3}$$

The QEP can be transformed into an equivalent generalized eigenvalue problem by adding the following transformation : let $\boldsymbol{Q} = \begin{bmatrix} \frac{\boldsymbol{\phi}^{EF}}{k} \\ \boldsymbol{\phi}^{EF} \end{bmatrix}$ then the final expression is

$$\begin{bmatrix} 0 & I \\ -\mathbf{K}_2^{-1}\mathbf{K}_0 & -\mathbf{K}_2^{-1}\mathbf{K}_1 \end{bmatrix} \begin{bmatrix} \frac{\boldsymbol{\phi}^{EF}}{k} \\ \boldsymbol{\phi}^{EF} \end{bmatrix} = k \begin{bmatrix} \frac{\boldsymbol{\phi}^{EF}}{k} \\ \boldsymbol{\phi}^{EF} \end{bmatrix} \tag{4}$$

(4) depends on the frequency and it is solved for each frequency to obtain $(k, \boldsymbol{\phi}^{EF})$ couples. To reduce computational time and avoid numerical problems (paragraph 2.5), a system reduction is introduced below (paragraph 2.3).

The number of wavenumbers is equal to $2 \times 3N$. They appear in conjugate pairs which correspond to the same waveshape in opposite directions.

Finally, the displacement of section $\tilde{\boldsymbol{u}}$ is written as follow :

$$\tilde{\boldsymbol{u}}(z) = \sum_{j}^{N_m} \boldsymbol{\alpha}_j e^{k_j z} \boldsymbol{\phi}_j + \boldsymbol{\beta}_j e^{-k_j z} \boldsymbol{\psi}_j \tag{5}$$

where the˜symbolizes the projection of the vector on the basis. $(\boldsymbol{\alpha}_j, k_j, \boldsymbol{\phi}_j)$ are associated to waves propagating in the negative direction and $(\boldsymbol{\beta}_j, -k_j, \boldsymbol{\psi}_j)$ those propagating in the positive direction. To simplify the notation, $\tilde{\boldsymbol{u}}(z)$ can be written as:

$$\tilde{\boldsymbol{u}}(z) = \boldsymbol{\phi} \boldsymbol{\Delta}(z) \boldsymbol{\alpha} + \boldsymbol{\psi} \boldsymbol{\Delta}^{-1}(z) \boldsymbol{\beta} \tag{6}$$

where $\boldsymbol{\phi}$, $\boldsymbol{\psi}$, $\boldsymbol{\alpha}$ and $\boldsymbol{\beta}$ are matrices whose columns are $\boldsymbol{\phi}_i$, $\boldsymbol{\psi}_i$, $\boldsymbol{\alpha}_i$ and $\boldsymbol{\beta}_i$. $\boldsymbol{\Delta}(z)$ is a diagonal matrix composed by the $e^{k_j z}$.

2.3 Projection basis using a second order Arnoldi method

Numerical problems and computational efficiency requirement (cf. §2.5) impose an adapted reduction model technique. A second order Arnoldi method allows to simultaneously create an orthonormal basis, reduce ill condition number and computational time.

The Arnoldi method is an iterative algorithm based on linear algebra and Krylov subspaces. It allows to solve complex eigenvalues problems using a reduction model technique. It integrates Gram-Schmidt orthogonalization which allows to work on an orthonormal basis.

The second order Arnoldi method (SOAR) presented in [19], is an adaptation of this method to solve quadratic eigenvalue problems (Eq. (3)). It computes an orthonormal basis which is projected on $\mathbf{K}_0$,$\mathbf{K}_1$ and $\mathbf{K}_2$. Then, the reduced model is solved. Finally, the reduced solution is projected on the basis to obtain the solution.

SOAR calculates the largest magnitude eigenvalues and their corresponding eigenvectors. In our case, the smallest ones must be calculated. Consequently, assuming $k \neq 0$ the following substitution is done : $\mu = \frac{1}{k}$

$$\left[\mathbf{K}_2 \left(\frac{1}{\mu}\right)^2 + \mathbf{K}_1 \frac{1}{\mu} + \mathbf{K}_0\right] \phi = 0 \Leftrightarrow \left[\mathbf{K}_0 \mu^2 + \mathbf{K}_1 \mu + \mathbf{K}_2\right] \phi = 0 \tag{7}$$

Moreover, this method imposes to inverse $\mathbf{K}_0$. This latter is always nonsingular because it is positive definite. Input parameters are $A_1 = -\mathbf{K}_0^{-1}\mathbf{K}_1$, $B_1 = -\mathbf{K}_0^{-1}\mathbf{K}_2$ and an initial vector u_0.

Algorithm 1 is the procedure to apply the SOAR. It generates an orthonormal basis $\{q_1, q_2, ..., q_n\}$ of the second order Krylov subspace $\mathscr{G}_N(A_1, B_1, u_0)$.

Algorithm 1 SOAR procedure

Require: $n > 0$ & $u_0 \neq 0$
  $\mathrm{q_1} = \frac{\mathrm{u_0}}{||\mathrm{u_0}||_2}$
  $\mathrm{p_1} = 0$
  for $j = 1 \rightarrow n$ **do**
    $\mathrm{r} = \mathrm{A_1 q_j} + \mathrm{B_1 p_j}$
    $\mathrm{s} = \mathrm{q_j}$
    for $i = 1 \rightarrow \mathrm{j}$ **do**
      $\mathrm{t_{ij}} = \mathrm{q_j^T r}$
      $\mathrm{r} = \mathrm{r} - \mathrm{q_i t_{ij}}$
      $\mathrm{s} = \mathrm{s} - \mathrm{p_i t_{ij}}$
    end for
    $\mathrm{t_{i+1j}} = ||\ \mathrm{r}\ ||_2$
    if $\mathrm{t_{j+1j}} = 0$ **then**
      return
    end if
    $\mathrm{q_{j+1}} = \frac{\mathrm{r}}{\mathrm{t_{j+1j}}}$
    $\mathrm{p_{j+1}} = \frac{\mathrm{s}}{\mathrm{t_{j+1j}}}$
  end for

SOAR is applied on Eq. 3 to create the basis. Effectiveness of this method will be shown in paragraph 3.

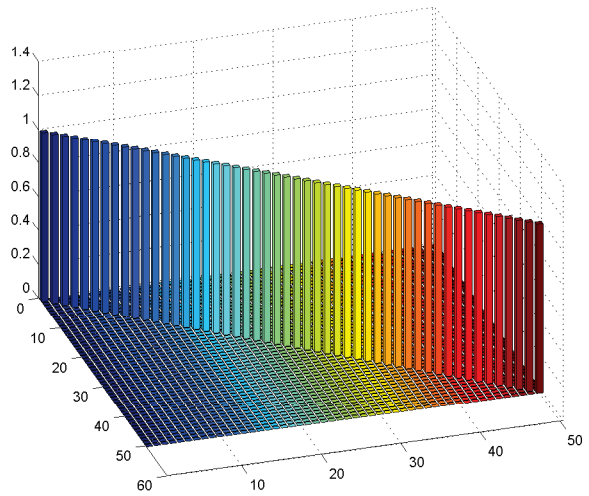

Fig. 2: Mac visualisation of the SOAR basis

2.4 Modeling the support

The support is modelled with a mass-spring system (Fig. 3). The sleeper is represented by a rigid mass. Six springs with hysteretic damping for the six sleeper's degrees of freedom are used to model the ballast

(3 translations and 3 rotations). To take into account pad width, this latter is modelled with N_n groups of springs. N_n is the number of nodes located on the rail foot (touching the pad). Each group models three traction springs in the three axis directions.

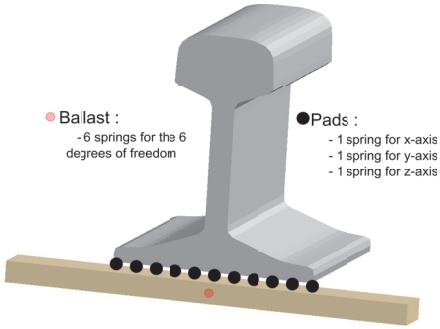

Fig. 3: support modelisation

The support impedance matrix $\boldsymbol{A}_p$ which appears in (2) is modelled thanks to the following steps :

- Sleeper Equilibrium to find its displacement
- Reinjecting it into the equation modelling the force exerted by the pad springs
- Projection on the basis

2.5 Free waves in infinite rail with a periodic support

Stress and displacement continuity between the element i and $i+1$ allows to calculate free waves in the complete system.

$$\begin{cases} \mathbf{G}_p(0) = -\mathbf{G}_p(L) \\ \tilde{\boldsymbol{u}}(z_i = L) - \tilde{\boldsymbol{u}}(z_{i+1} = 0) = 0 \end{cases} \tag{8}$$

Substituting the $\tilde{\boldsymbol{u}}$ expression given in (6) leads to the following equations:

$$\begin{cases} (\boldsymbol{\phi}\boldsymbol{\alpha}^{i+1} + \boldsymbol{\psi}\boldsymbol{\beta}^{i+1}) - (\boldsymbol{\phi}\boldsymbol{\Delta}\boldsymbol{\alpha}^{i} + \boldsymbol{\psi}\boldsymbol{\Delta}^{-1}\boldsymbol{\beta}^{i}) = 0 \\ (\boldsymbol{\phi}\boldsymbol{K}\boldsymbol{\alpha}^{i+1} + \boldsymbol{\psi} - \boldsymbol{K}\boldsymbol{\beta}^{i+1}) - (\boldsymbol{\phi}\boldsymbol{K}\boldsymbol{\Delta}\boldsymbol{\alpha}^{i} + \boldsymbol{\psi} - \boldsymbol{K}\boldsymbol{\Delta}^{-1}\boldsymbol{\beta}^{i}) - \mathbf{B}_3^{-1}\boldsymbol{A}_p(\boldsymbol{\phi}\boldsymbol{\Delta}\boldsymbol{\alpha}^{i} + \boldsymbol{\psi}\boldsymbol{\Delta}^{-1}\boldsymbol{\beta}^{i}) = 0 \end{cases} \tag{9}$$

where $\boldsymbol{\Delta} = \boldsymbol{\Delta}(L)$ and $\boldsymbol{K}$ is the diagonal matrix of the k_j. The unknown parameters are $\boldsymbol{\alpha}$ and $\boldsymbol{\beta}$. The equation system can be written as follows:

$$\boldsymbol{H}\boldsymbol{\gamma}^{i+1} - (\boldsymbol{H} + \boldsymbol{A})\boldsymbol{\Lambda}\boldsymbol{\gamma}^{i} = 0 \Leftrightarrow (\boldsymbol{I} + \boldsymbol{H}^{-1}\boldsymbol{A})\boldsymbol{\Lambda}\boldsymbol{\gamma}^{i} = \boldsymbol{\gamma}^{i+1} \tag{10}$$

with

$$\boldsymbol{H} = \begin{bmatrix} \boldsymbol{\phi}\boldsymbol{K} & -\boldsymbol{\psi}\boldsymbol{K} \\ \boldsymbol{\phi} & \boldsymbol{\psi} \end{bmatrix}, \boldsymbol{A} = \begin{bmatrix} \mathbf{B}_3^{-1}\boldsymbol{A}_p\boldsymbol{\phi} & \mathbf{B}_3^{-1}\boldsymbol{A}_p\boldsymbol{\psi} \\ \mathbf{0} & \mathbf{0} \end{bmatrix}, \boldsymbol{\Lambda} = \begin{bmatrix} \boldsymbol{\Delta} & \mathbf{0} \\ \mathbf{0} & \boldsymbol{\Delta}^{-1} \end{bmatrix} \text{ and } \boldsymbol{\gamma} = \begin{bmatrix} \boldsymbol{\alpha} \\ \boldsymbol{\beta} \end{bmatrix}$$

To link waves between elements i and $i+1$, the periodicity hypothesis in the longitudinal direction and Floquet theorem are used: $\tilde{\boldsymbol{u}}^{i+1}(z) = \lambda\tilde{\boldsymbol{u}}^{i}(z)$. As $\boldsymbol{\gamma}^{i+1} = \boldsymbol{\lambda}\boldsymbol{\gamma}^{i}$, the system becomes

$$(\boldsymbol{I} + \boldsymbol{H}^{-1}\boldsymbol{A})\Lambda\boldsymbol{\gamma}^{i} = \lambda\boldsymbol{\gamma}^{i} \tag{11}$$

$\boldsymbol{T}\boldsymbol{\Lambda} = (\boldsymbol{I} + \boldsymbol{H}^{-1}\boldsymbol{A})\boldsymbol{\Lambda}$ is called transfer matrix which links waves from an element to the next one. Its size is $2N \times 2N$.

The eigenvalue problem (11) resolution allows to determine free waves in an infinite rail with a periodic support. However, this matrix is ill conditionned because it has eigenvalues with a large modulus ratio due to e^{kL} and e^{-kL} terms associated with strongly decaying waves. In [7], an algorithm mitigating this problem is suggested. It solves the eigenvalue problem $\boldsymbol{T}\boldsymbol{\Lambda} + \boldsymbol{\Lambda}^{-1}\boldsymbol{T}$ without directly inverting $\boldsymbol{\Lambda}$.

2.6 Track response

Two cases are considered: a force is located above the sleeper (between two sections) and a force is located on the genereric element. In both cases, a force $\boldsymbol{F}_r$ is add to Eq. 9. Characteristic waves are defined by linear combinations of free wave eigenvectors.

In the first case (Fig. 4), waves travelling in the positive direction are assumed to be equal to zero in the element i. Respectively, those travelling in the negative direction are assumed to be equal to zero in the element $i+1$. Without this hypothesis, energy would tend to infinity at infinity.

$$\begin{array}{ll} \boldsymbol{\alpha}^i = \boldsymbol{\alpha\epsilon} & \boldsymbol{\alpha}^{i+1} = \boldsymbol{\alpha\zeta} \\ \boldsymbol{\beta}^i = \boldsymbol{\beta\epsilon} & \boldsymbol{\beta}^{i+1} = \boldsymbol{\beta\zeta} \end{array} \tag{12}$$

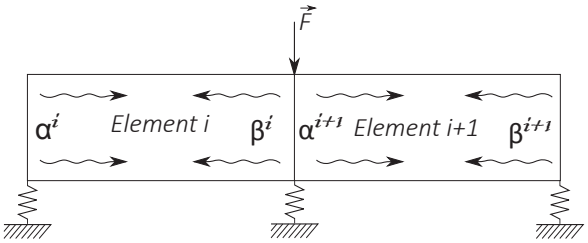

Fig. 4: Wave propagation due to a force between two elements

Reinjecting these expressions in the equation allows to calculate the response :

$$\tilde{\boldsymbol{u}}^i(L) = \left(\boldsymbol{\phi\Delta\alpha} + \boldsymbol{\psi\Delta}^{-1}\boldsymbol{\beta}\right)\left[\boldsymbol{A}_1 + \mathbf{B}_3\boldsymbol{A}_p\boldsymbol{A}_2 - \boldsymbol{A}_3{\boldsymbol{A}_4}^{-1}\boldsymbol{A}_2\right]^{-1}\mathbf{B}_3^{-1}\mathbf{F}_r \tag{13}$$

with

$$\begin{array}{ll} \boldsymbol{A}_1 = \left(\boldsymbol{\phi K\Delta\alpha} - \boldsymbol{\psi K\Delta}^{-1}\boldsymbol{\beta}\right) & \boldsymbol{A}_2 = \left(\boldsymbol{\phi\Delta\alpha} + \boldsymbol{\psi\Delta}^{-1}\boldsymbol{\beta}\right) \\ \boldsymbol{A}_3 = \left(\boldsymbol{\phi K\alpha} - \boldsymbol{\psi K\beta}\right) & \boldsymbol{A}_4 = \left(\boldsymbol{\phi\alpha} + \boldsymbol{\psi\beta}\right) \end{array} \tag{14}$$

We work on a reduced basis. Calculation of the receptance $\boldsymbol{R}_{ecept} = \boldsymbol{UF}^{-1}$ is done projecting the model on the basis. Columns of the basis corresponding to the node and the direction of the displacement $\boldsymbol{U}_D$ and the force $\boldsymbol{U}_F$ are selected. Finally the receptance calculates as follows :

$$\boldsymbol{R}_{ecept} = \boldsymbol{U}_D^T\left(\boldsymbol{\phi\Delta\alpha} + \boldsymbol{\psi\Delta}^{-1}\boldsymbol{\beta}\right)\left[\boldsymbol{A}_1 + \mathbf{B}_3\boldsymbol{A}_p\boldsymbol{A}_2 - \boldsymbol{A}_3{\boldsymbol{A}_4}^{-1}\boldsymbol{A}_2\right]^{-1}\mathbf{B}_3^{-1}\boldsymbol{U}_F \tag{15}$$

In the other case (cf. Fig. 5), the force produces two groups of waves. The first ones travelling to portion located on the left of the excitation and those for the portion on the right.

$$\begin{array}{ll} \boldsymbol{\alpha}^g = \boldsymbol{\alpha\epsilon} & \boldsymbol{\alpha}^d = \boldsymbol{\alpha\zeta} \\ \boldsymbol{\beta}^g = \boldsymbol{\beta\epsilon} & \boldsymbol{\beta}^d = \boldsymbol{\beta\zeta} \end{array} \tag{16}$$

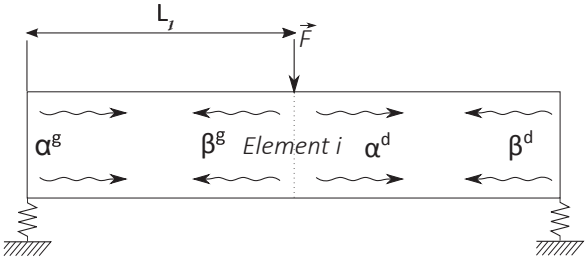

Fig. 5: Waves produced by a force on a generic element

Receptance is calculated with the same reasoning as previously:

$$\boldsymbol{R}_{ecept} = \boldsymbol{U}_D^T\left(\boldsymbol{\phi\Delta}_{L_1}\boldsymbol{\alpha} + \boldsymbol{\psi\Delta}_{L_1}^{-1}\boldsymbol{\beta}\right)\left[\boldsymbol{A}_1 - \boldsymbol{A}_3{\boldsymbol{A}_4}^{-1}\boldsymbol{A}_2\right]^{-1}\mathbf{B}_3^{-1}\boldsymbol{U}_F \tag{17}$$

with

$$\begin{array}{ll} \boldsymbol{A}_1 = \left(\boldsymbol{\phi K\Delta}_{L_1}\boldsymbol{\alpha} - \boldsymbol{\psi K\Delta}_{L_1}^{-1}\boldsymbol{\beta}\right) & \boldsymbol{A}_2 = \left(\boldsymbol{\phi\Delta}_{L_1}\boldsymbol{\alpha} + \boldsymbol{\psi\Delta}_{L_1}^{-1}\boldsymbol{\beta}\right) \\ \boldsymbol{A}_3 = \left(\boldsymbol{\phi K\Delta}_{L_1}\boldsymbol{\alpha} - \boldsymbol{\psi K\Delta}_{L_1}^{-1}\boldsymbol{\beta}\right) & \boldsymbol{A}_4 = \left(\boldsymbol{\phi\Delta}_{L_1}\boldsymbol{\alpha} + \boldsymbol{\psi\Delta}_{L_1}^{-1}\boldsymbol{\beta}\right) \end{array}$$

3. RESULTS ANALYSIS

As explained in the paragraph 2.2 a projection basis is created by selecting the eigenvectors corresponding to smaller wavenumbers. This basis depends on the number of selected modeshapes and the frequency chosen. The influence of those parameters will be analyzed.

System material properties used in this section are given in Table 1. UIC60 rail is meshed with linear triangular elements. A convergence study guarantees a good approximation for 137 nodes.

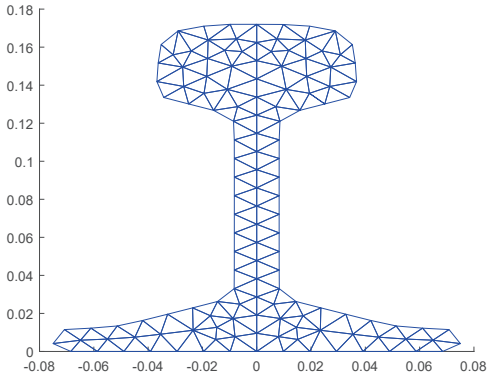

Fig. 6: Rail cross section mesh - 137 nodes

	Vertical	Lateral	Longitudinal
Rail : UIC60			
Young modulus [MPa]	2.1e5		
Shear coefficient [-]	0.3		
Rail loss factor [-]	0.001		
Density [$kg.m^{-1}$]	7850		
Pads :			
Traction stifness [$N.m^{-1}$]	4e8	1.2e8	8e8
Traction loss factor [-]	0.2	0.2	0.2
Mass (1/2 sleeper) [kg]	122		
Distance between sleepers [m]	0.6		
Ballast :			
Traction stifness [$N.m^{-1}$]	9e7	1e8	9.5e8
Traction loss factor [-]	0.8	0.8	0.2
Torsion stifness [$N.m^{-1}$]	2.5e8	2e8	2e8
Torsion loss factor [-]	0.8	0.8	0.8

Table 1: Input parameters

3.1 Influence on the choice of the number of selected modes

Influence of the number of selected modes on accelerance is shown in figures 7 and 8. Lateral accelerance converges with few selected modes. However, the second mode takes more time to converge. This frequency corresponds with rail and ballast vibrating in phase opposition. Consequently, the support model needs a sufficiently large basis to converge. To study convergence of this eigenfrequency value, relative difference in percentage ($|\frac{freq_i - freq_{conv}}{freq_{conv}}| * 100$) is considered (cf. Fig. 9). $freq_{conv}$ is the 2^{nd} eigenfrequency value for 68 selected modes . It shows the system convergence.

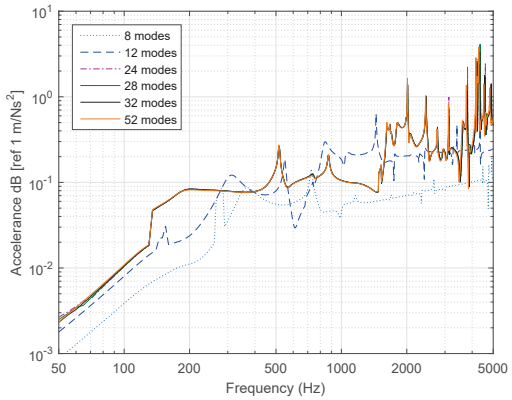

Fig. 7: Lateral accelerance at mid-span - influence of the SOAR basis size

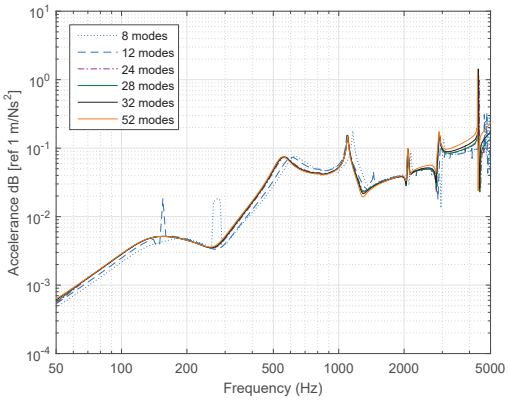

Fig. 8: Vertical accelerance at mid-span - influence of the SOAR basis size

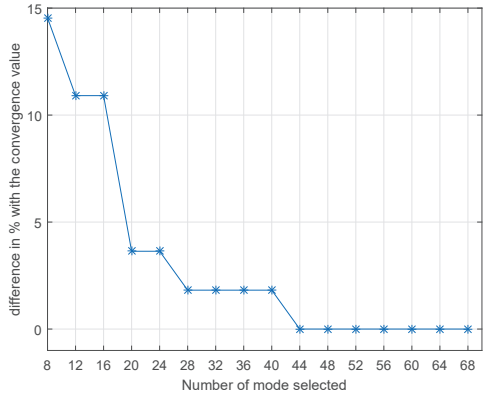

Fig. 9: Deviation in % of the 2^{nd} eigenvalue for the vertical accelerance at mid-span

3.2 Influence on the frequency chosen to create the basis

In [3], Gavric demonstrates that rail modeshape of a given wave depends on frequency. Consequently, basis depends on frequency. To check influence of the basis, accelerances are calculated with basis at different frequencies. Figures 10 to 13 allow to prove that there is no influence on accelerance results. Consequently, SOAR doesn't induce stability problems.

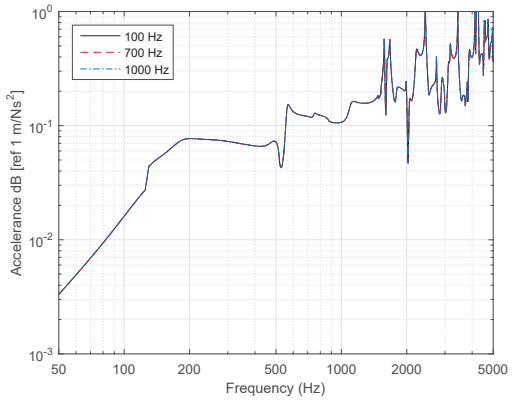

Fig. 10: Lateral accelerance above a sleeper - influence of the frequency to create the basis

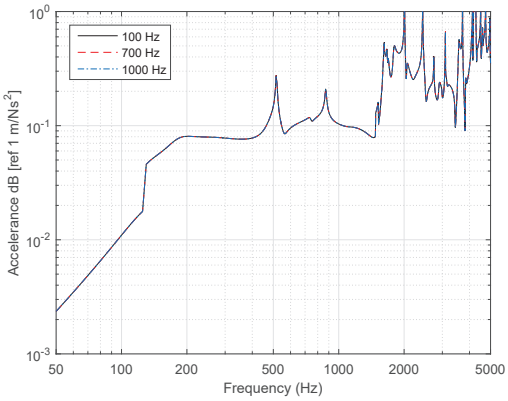

Fig. 11: Lateral accelerance at mid-span - influence of the frequency to create the basis

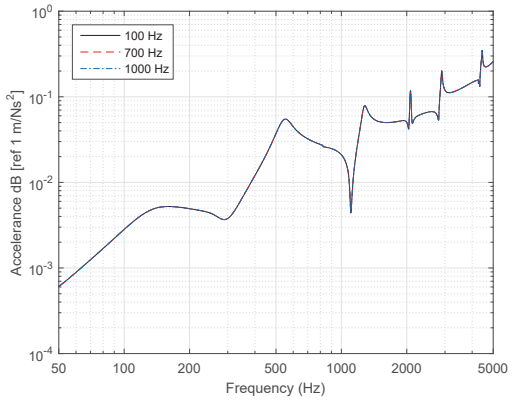

Fig. 12: Vertical accelerance above a sleeper - influence of the frequency to create the basis

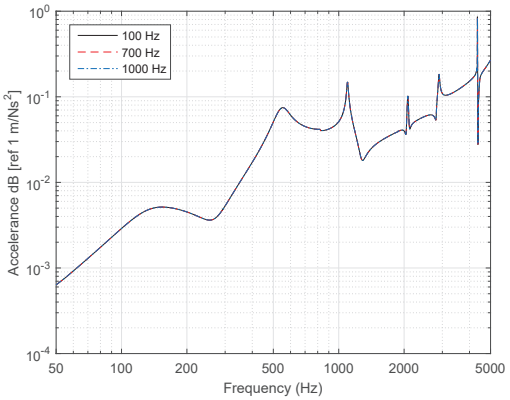

Fig. 13: Vertical accelerance at mid-span - influence of the frequency to create the basis

4. COMPARISON WITH EXPERIMENTAL RESULTS

To validate the model, simulations are compared with experimental results. Experimental data were driven from a test campaign carried out in 2005 [20]. Accelerances are measured using an impact hammer and an accelerometer located below the rail foot (cf. Fig. 14). Vertical excitation is located on the upper surface of rail head. Lateral excitation is located on the external face of the rail head. Measuring points are at midway between two sleepers (at the middle of the element). Coherence curves validate measurements between 100 and 5000 Hz.

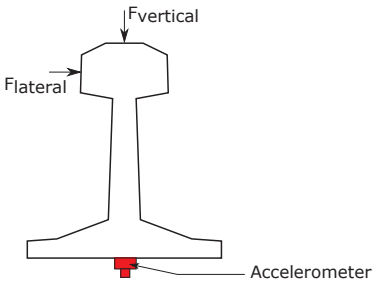

Fig. 14: Hammer excitation and accelerometer location

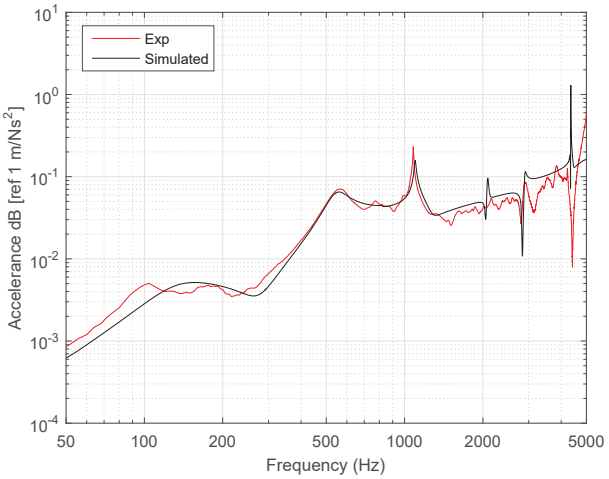

Fig. 15: Vertical accelerance at mid-span - Comparison between experimental and simulated results

Figures 15 and 16 compare experimental results against simulation. Vertical accelerance curves are very close which allows to validate the model. However, for the lateral accelerance, there is a gap at 130 Hz. Below this frequency the accelerance is underestimated. Above this frequency, curves match very well.

Consequently, the model is validated at each frequency for the vertical excitation and above 130 Hz for lateral excitation.

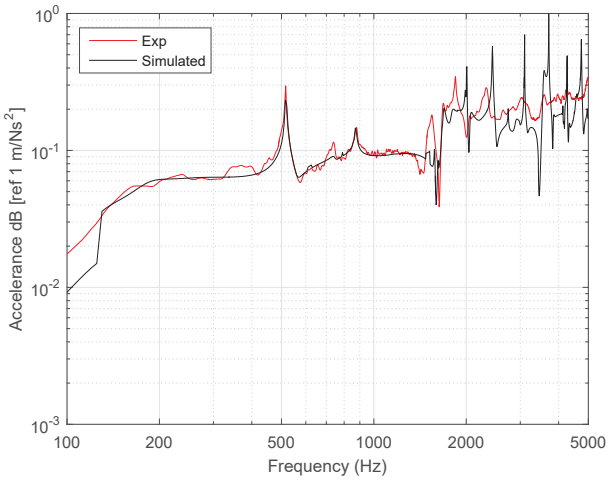

Fig. 16: Lateral accelerance at mid-span - Comparison between experimental and simulated results

5. CONCLUSION

In this paper, a computationally efficient method modeling rail vibration response is presented. This model allows to take into account infinite dimension of the rail in the longitudinal direction, its cross section deformation and the periodic support.

This method introduced in [7, 8], presents numerical problems linked to e^{kL}/e^{-kL} ratio in the transfer matrix (paragraph 2.5). To overcome these numerical problems, a model reduction is done. However, it reveals instability at low frequency due to the non-orthogonality of the basis.

SOAR is proposed to overcome these problems. It allows, thanks to an orthonormal basis creation, to remove these instabilities. In addition, a comparison with experimental results validate the model.

The very promising results open a series of further development removing some simplification hypothesis.

In this work, Support is modelled with a simple mass-spring system. To take into account the sleeper deformation, it would be interesting to model it thank finite elements or finite elements/ spring. Support is applied on one point in the space. However, sleeper width is around 25 cm. Creating a generic element taking into account this dimension could be developed.

Moreover, at high frequency, pick amplitude is overestimated (cf. Fig. 16). This is due to the nonlinear behavior of the pad which is not taken into account. A model to better predict rail response at high frequency should be developed

REFERENCES

[1] Estelle Bongini. *Modèle acoustique global et synthèse sonore du bruit d ' un véhicule : application aux véhicules ferroviaires*. PhD thesis, Universié de Provence, 2008, (in french).

[2] MARIA A Heckl. Coupled Waves on a Periodically Supported Timoshenko Beam. *Journal of Sound and Vibration*, 252(5):849–882, 2002.

[3] L. Gavrić. Computation of propagative waves in free rail using a finite element technique. *Journal of Sound and Vibration*, 185(3):531–543, 1995.

[4] Takahiro Hayashi, Won Joon Song, and Joseph L. Rose. Guided wave dispersion curves for a bar with an arbitrary cross-section, a rod and rail example. *Ultrasonics*, 41(3):175–183, 2003.

[5] C. M. Nilsson, C. J C Jones, D. J. Thompson, and J. Ryue. A waveguide finite element and boundary element approach to calculating the sound radiated by railway and tram rails. *Journal of Sound and Vibration*, 321(3-5):813–836, 2009.

[6] X. Sheng, C.J.C. Jones, and D.J. Thompson. Modelling ground vibration from railways using wavenumber finite- and boundary-element methods. *Proceedings of the Royal Society A: Mathematical, Physical and Engineering Sciences*, 461(2059):2043–2070, 2005.

[7] L. Gry. *Modélisation du comportement dynamique d'une voie TGV pour la réduction du bruit de roulement*. PhD thesis, 1995, (in french).

[8] L. Gry. Dynamic Modelling of Railway Track Based on Wave Propagation. *Journal of Sound and Vibration*, 195(3):477–505, 1996.

[9] D. Duhamel, B. R. Mace, and M. J. Brennan. Finite element analysis of the vibrations of waveguides and periodic structures. *Journal of Sound and Vibration*, 294(1-2):205–220, 2006.

[10] C. Droz, J. P. Lainé, M. N. Ichchou, and G. Inquiété. A reduced formulation for the free-wave propagation analysis in composite structures. *Composite Structures*, 113(1):134–144, 2014.

[11] L. Gavrić. Finite element computation of dispersion propertiesof thin-walled waveguides.pdf, 1994.

[12] L. Houillon, M. N. Ichchou, and L. Jezequel. Wave motion in thin-walled structures. *Journal of Sound and Vibration*, 281(3-5):483–507, 2005.

[13] M. N. Ichchou, J. M. Mencik, and W. Zhou. Wave finite elements for low and mid-frequency description of coupled structures with damage. *Computer Methods in Applied Mechanics and Engineering*, 198(15-16):1311–1326, 2009.

[14] Brian R Mace, Denis Duhamel, Michael J Brennan, and Lars Hinke. Finite element prediction of wave motion in structural waveguides. *The Journal of the Acoustical Society of America*, 117(May 2005):2835–2843, 2005.

[15] Jamil M. Renno and Brian R. MacE. On the forced response of waveguides using the wave and finite element method. *Journal of Sound and Vibration*, 329(26):5474–5488, 2010.

[16] Y. Waki, B. R. Mace, and M. J. Brennan. Numerical issues concerning the wave and finite element method for free and forced vibrations of waveguides. *Journal of Sound and Vibration*, 327(1-2):92–108, 2009.

[17] W. J. Zhou and M. N. Ichchou. Wave propagation in mechanical waveguide with curved members using wave finite element solution. *Computer Methods in Applied Mechanics and Engineering*, 199(33-36):2099–2109, 2010.

[18] Wenjin J. Zhou, Mohamed N. Ichchou, and Olivier Bareille. Finite element techniques for calculations of wave modes in one-dimensional structural waveguides. *Structural Control and Health Monitoring*, (May 2011):n/a–n/a, 2011.

[19] Zhaojun Bai and Yangfeng Su. SOAR: A second-order Arnoldi method for the solution of the quadratic eigenvalue problem. *SIAM Journal on Matrix Analysis and Applications*, 26(3):640–659, 2005.

[20] F. Letourneaux and G. Gerault. Projet de recherche E03642 : absorbeurs dynamiques sur rails, 2005, (in french).